

## Particle velocity fluctuations and hydrodynamic self-diffusion of sedimenting non-Brownian spheres

H. Nicolai and B. Herzhaft

*Laboratoire de Physique et Mécanique des Milieux Hétérogènes, URA 857 au CNRS, ESPCI, 10 rue Vauquelin, 75231 Paris Cedex 05, France*

E. J. Hinch

*Department of Applied Mathematics and Theoretical Physics, University of Cambridge, Silver Street, Cambridge, CB39EW, United Kingdom*

L. Oger<sup>a)</sup> and E. Guazzelli

*Laboratoire de Physique et Mécanique des Milieux Hétérogènes, URA 857 au CNRS, ESPCI, 10 rue Vauquelin, 75231 Paris Cedex 05, France*

(Received 2 March 1994; accepted 22 September 1994)

The motion of non-Brownian spheres settling in the midst of a suspension of like spheres has been experimentally studied under creeping flow conditions. A few glass spheres, marked with a thin coating of silver, were tracked in a suspension of unmarked glass spheres, made optically transparent by matching the index of refraction of the suspending fluid to that of the glass spheres. Particles were tracked with a real time digital imaging processing system. Particle trajectories were examined in the bulk region of the suspension for particle volume fractions ranging from 0% to 40% in 5% steps. Statistical analyses of local particle velocities yield the mean settling velocity, the RMS of the fluctuations of the vertical and horizontal particle velocity and the particle velocity autocorrelation functions. The long time fluctuating particle motion is demonstrated to be diffusive in nature. Vertical and horizontal correlation times and self-diffusivities are found as a function of particle volume fraction, and a strongly anisotropic diffusion noted. © 1995 American Institute of Physics.

### I. INTRODUCTION

The sedimentation of particles in a viscous fluid is one of the oldest engineering processes used to segregate particles from fluid, as well as to separate particles of different densities or sizes. Although some progress has been made in understanding the mean properties of a sedimenting suspension, such as the mean particle sedimentation velocity, less is known about particle velocity fluctuations. One of the essential difficulties lies in the incomplete understanding of the long range multibody hydrodynamic interactions, especially under the usual circumstance of concentrated suspensions.

Throughout we shall confine our attention to suspensions composed of non-Brownian rigid spherical particles of equal size and density sedimenting in a Newtonian fluid under creeping flow conditions. If the suspension is infinitely dilute, the particle velocity is equal to Stokes' settling velocity,  $V_s = 2 \Delta \rho a^2 g / 9 \eta$ , where  $\Delta \rho = \rho_p - \rho_f$  is the difference between the density of the particles and that of the fluid,  $a$  is the particle radius,  $\eta$  is the fluid viscosity, and  $g$  is the acceleration due to gravity. As soon as the particle concentration is increased, the motion of an individual sphere settling in the midst of a suspension of like spheres is affected by the

presence of the other particles in the fluid. In a uniformly concentrated suspension, the mean particle sedimentation velocity is noticeably smaller than the Stokes' velocity, and is given by  $\langle V \rangle = f(\phi) V_s$ .<sup>1</sup> Here and in the remainder of this paper,  $\langle \rangle$  denotes an ensemble average. The function  $f(\phi)$  is known as the hindered settling function and is a monotonically decreasing function of the volume fraction of particles in the suspension,  $\phi$ . There are three experimental methods for determining the hindered settling function. The first method is to measure the fall velocity of the interface at the top of the sedimenting suspension.<sup>2-4</sup> The second is to measure the variation with time of the total number of particles above a fixed horizontal plane in the interior of the suspension.<sup>5</sup> The third is to measure the settling velocities of a marked particle in the bulk suspension region and to determine an average settling speed.<sup>6</sup> The most commonly found empirical law is that proposed by Richardson and Zaki,<sup>7</sup>  $f(\phi) = (1 - \phi)^n$ , where a value of  $n$  of the order of 5 usually represents experimental results for small particle Reynolds numbers,  $Re = \rho_f V_s a / \eta$ .<sup>1</sup>

Although the suspension may be macroscopically homogeneous, hydrodynamic interactions lead to changes in the suspension microstructure, and hence to changes in the particle velocities during the settling process. Consequently, even in a monodisperse suspension, the instantaneous particle velocities fluctuate about the mean sedimentation velocity during the sedimentation process. Particles settle with dis-

<sup>a)</sup>Present address: Groupe Matière Condensée et Matériaux, URA 804 au CNRS, Université de Rennes I, Campus de Beaulieu, 35042 Rennes Cedex, France.

tributions of velocities both parallel and perpendicular to the mean velocity. The variance (or the standard deviation) of the velocity distribution is the simplest measure of the particle velocity fluctuations. The velocity fluctuations can lead to randomly fluctuating particle motions, which have a long time behavior characteristic of a diffusion process known as hydrodynamic self-diffusion. Large particle velocity fluctuations, ranging up to 46% of the mean, have been observed experimentally by Ham and Homsy<sup>6</sup> during measurements of vertical velocities of a marked particle in quiescent sedimenting suspensions. The long time behavior of the sedimentation velocity variance was shown to be characteristic of a diffusion process, and estimates of vertical self-diffusion coefficients were determined for particle concentrations ranging from 2.5% to 10%. Dimensionless self-diffusivities (based on length scale  $a$  and time scale  $a/V_S$ ) were found to be  $O(1)$ . In an experiment using a multiple light scattering technique and a fluidized bed,<sup>8</sup> the fluctuations in the sedimentation velocity were found comparable to the mean sedimentation velocity at concentration ranging from 15% to 30%, but to decrease faster than the mean at higher concentration.

It still remains a challenge to compute theoretically the effect of particle interactions on the mean sedimentation velocity and its variance over the entire range of particle concentrations. Even for dilute suspensions, the direct summing of long range particle pair interactions leads to a divergent integral. In order to overcome this difficulty, Batchelor<sup>9</sup> introduced a renormalization method and found the first correction to the mean sedimentation velocity for a dilute, random, monodisperse suspension:  $\langle V \rangle = V_S(1 - 6.55\phi)$ . Other methods have been developed to avoid this divergence problem,<sup>10-14</sup> and the departure from unity of the hindered function has been shown to depend strongly upon the suspension microstructure.<sup>1</sup> However, Batchelor's renormalization does not resolve divergence difficulties associated with the velocity variance. For dilute, random suspensions, Cafilisch and Luke<sup>15</sup> showed that the velocity variance and the self-diffusivity diverge when the characteristic dimension of the settling vessel is increased. A scaling argument for the divergence of the velocity fluctuations produced by the density fluctuations has been also proposed by Hinch.<sup>16</sup> A resolution of this divergence has been suggested by Koch and Shaqfeh<sup>17</sup> by introducing a Debye-like screening of particle velocity disturbance, which assumes that the integral of the pair distribution function (their 2.14) is exactly  $-1$ . The screening leads to particle velocity variance and self-diffusivity that are finite.

Numerical simulations seem to provide fundamental insights into the sedimentation process.<sup>18-21</sup> The difficulty here is again to compute the multibody hydrodynamic interactions. Current state of the art numerical computations suffer from two serious limitations. First, the number of particles is fairly small in some numerical simulations, and therefore size effects can become important, especially with low particle concentrations. Second, hydrodynamic interactions are only computed at the lowest approximations (i.e., particle pair interactions) in some computations, and thus features of the suspension arising from multiparticle interactions are

poorly approximated. Such interactions may not be negligible for any particle concentration.

On a macroscopic scale, particle velocity fluctuations can lead to diffusion phenomena, and thus are important for the understanding of mixing processes that inhibit separation. The observed spreading of the upper interface of a sedimenting suspension has been attributed to a hydrodynamic gradient diffusion and gradient diffusivities have been estimated. Although such a gradient diffusivity and the self-diffusivity of the random walk in a uniform suspension are not expected to be the same, dimensionless gradient diffusivities reported by Davis and Hassen<sup>2</sup> are of the same order of magnitude as dimensionless self-diffusivities estimated by Ham and Homsy.<sup>6</sup> More recent experiments give much larger values of gradient diffusivities.<sup>4</sup> In a slightly different context of fluidized beds, Batchelor<sup>22</sup> argued that hydrodynamic gradient diffusion plays the role of a stabilization mechanism against the growth of concentration wave instability. Stable regions of fluidization have been found experimentally, and estimates of gradient diffusivities have been deduced from Batchelor's stability criterion.<sup>23</sup> Since these estimates were obtained at the instability threshold, and therefore, for large particle concentrations, no comparison can be made with the above experimental results that were obtained at low concentrations. Finally, we should mention the related phenomenon of shear-induced hydrodynamic diffusion for which diffusivities in sheared monodisperse suspensions of spheres have been determined experimentally.<sup>24,25</sup>

Our objective in this work was to measure particle velocity fluctuations and to analyze the long time behavior of the randomly fluctuating particle motion in the bulk region of sedimenting suspensions for a wide range of particle volume fractions up to 40%. To achieve this objective, a few glass spheres, marked with a thin coating of silver, were tracked in a suspension of unmarked glass spheres, made optically transparent by matching the index of refraction of the suspending fluid to that of the glass spheres. This index matching technique has been adapted from that of Ham and Homsy.<sup>6</sup> Small particle tracking was performed with a real time digital imaging processing system. Local particle velocities, both parallel and perpendicular to gravity, were then deduced. Statistical analyses of the data yield the mean settling velocity, the vertical and horizontal particle velocity fluctuations, and the particle velocity autocorrelation functions. It was then possible to verify whether the long time behaviors of fluctuating vertical and horizontal particle motions were characteristic of a diffusion process.

The present paper is organized as follows. The experimental techniques are presented in Sec. II. In Sec. III we describe the statistical methods applied to analyze the experimental data. The experimental results are given in Sec. IV and discussed in Sec. V.

## II. EXPERIMENTAL TECHNIQUES

### A. Particles and fluid

Following Ham and Homsy,<sup>6</sup> the fluid and particles used in our experiments were chosen to meet several criteria. First, fluid and particles were chosen to have the same index

of refraction so that marked particles could be tracked in optically transparent suspensions. Second, the fluid was to be viscous enough to provide a small particle Reynolds number. Third, particle size was to be large enough to enable precise tracking of the marked particles. This last criterion also ensured that Brownian effects were negligible for all experiments.

The particles were glass beads with index of refraction  $1.5190 \pm 0.0002$ . The beads that were supplied presieved were further carefully resieved between two meshes having openings of 710 and 800  $\mu\text{m}$ . The particle size distribution was analyzed by using a CCD camera and a digital imaging system (see Sec. II C for further information regarding the digital imaging system). From measurements of the projected bead surfaces, the particle diameter distribution was found to be approximately Gaussian with a mean particle diameter of 788  $\mu\text{m}$  and a standard deviation of 34  $\mu\text{m}$ . The particle density was determined, using Archimedes' principle, by measuring the volume variation when a weighted amount of particles was introduced into 100  $\text{cm}^3$  of distilled water in a graduated vessel. The particle density was  $\rho_p = 2.53 \pm 0.02 \text{ g/cm}^3$ .

A fraction of the particles was selected and then uniformly silvered. The silvering process was performed by reduction of an ammonia solution of silver nitrate by an alcoholic solution of saccharose. The thin coating of silver did not modify the bead settling characteristics. The silvered particles were thus considered identical to the nonsilvered particles and easily tracked in the midst of a suspension of like particles.

The suspending fluid was an alkyl benzyl phthalate plasticizer, named Santicizer 278 and produced by Monsanto. To ensure a close index matching of the fluid with that of the glass beads, the laboratory room temperature was maintained at  $22 \pm 1 \text{ }^\circ\text{C}$  by using an air conditioner. At this temperature, the measured properties of this fluid are a refractive index of  $1.5190 \pm 0.0002$ , a viscosity of  $\eta = 13 \pm 2 \text{ P}$  and a density of  $\rho_f = 1.09 \pm 0.01 \text{ g/cm}^3$ . The fluid viscosity was measured with a rheometer, and its Newtonian behavior was also verified.

For this combination of particles and fluid, the particle Reynolds number,  $2aV_s\rho_f/\eta$ , was smaller than  $10^{-3}$ , and the Brownian Péclet number was very large.

## B. Experimental procedure

All of the experiments were performed in a rectangular, glass walled vessel having inner dimensions of  $50.00 \pm 0.05 \text{ cm}$  high and  $10.00 \pm 0.05 \text{ cm}$  by  $4.00 \pm 0.05 \text{ cm}$  in the cross section. The width of the vessel was uniform to within 0.05 cm. A vessel height of  $50.00 \pm 0.05 \text{ cm}$  was chosen to provide a long enough distance to reach the long time behavior. A vessel inner width of  $4.00 \pm 0.05 \text{ cm}$  was chosen to be small enough to avoid large convection currents, but large enough to avoid serious wall effects. To check whether a convection current existed in the vessel containing only the fluid, the trajectories of a few buoyant beads were examined. A small convection current due to a weak thermal gradient was noticed across the vessel. This convection current, which was less than  $10^{-5} \text{ cm/s}$ , is significantly less than the experimental error of particle velocity measurement (see Sec. III for a

further discussion). A further restriction on the width of the vessel comes from the difficulty of seeing a long way into the center of the suspension, despite the good optical matching.

Experiments were carried out by introducing weighted amounts of fluid and marked and unmarked particles into the vessel to reach the desired particle volume concentration. The concentrations were varied throughout the range  $0\% \leq \phi \leq 40\%$  in 5% steps. The experimental relative error in particle concentration measurements was 1.5%. The quantity of marked beads added to the unmarked beads was varied, depending upon the concentration. Typically, between 10–50 marked beads were added, respectively, for small and large concentrations.

During the experiments, the vessel was held in a fixed position on a rail, with the vessel walls oriented vertically within 0.05 cm. A CCD camera (512×512 pixels), which could slide vertically, was fixed on the same rail in front of the vessel. A set of halogen lamps were placed behind the vessel, producing a homogeneous illumination of the suspension. The intensity of the light, as well as the camera lens opening, were chosen to ensure the best contrast between the marked particles and the transparent suspension. The CCD camera was focused in the median plane of the vessel. The depth of field of the imaging system was the depth of the vessel. For most of the experiments, the size of a marked particle corresponded to approximately ten pixels. For large concentrations ( $\phi = 40\%$ ), a magnification was used, which made the particles approximately 20 pixels (see Sec. II C for further discussion regarding sampling problems). The CCD camera recorded trajectories of marked particles settling in a square window of approximately 6 cm×6 cm located in the middle of the vessel. The location of the recording window was chosen to be far from the sedimentation front and the sediment growth, as well as far from the vessel walls. For the smallest concentrations, the window was not long enough to obtain the long time behavior. In this case, two windows were used. A particle was tracked in an upper window, and then, when it reached the window bottom, the camera was suddenly slid down and the particle was tracked in a lower window, which had a small overlap with the upper window, thereby providing measurement continuity. This last procedure, used only when  $\phi \leq 10\%$ , was more tedious since only one particle could be tracked per experiment. For larger concentrations, a single window was used, and several particles could be tracked simultaneously in one experiment.

Each sedimentation experiment consisted of mixing the suspension and then tracking particle(s) inside the imaging window (or the two windows for the small concentrations). The procedure for each experiment was identical. The suspension was mixed with a small propeller fixed at the end of a shaft driven by a variable-speed drill motor. The propeller was moved randomly within the suspension for several minutes in order to obtain a uniform particle distribution throughout the suspension. Caution was taken not to entrain any air bubbles through the liquid–air interface. The suspension was then allowed to settle for a short time until a sedimentation front had time to form between the suspension and the clear fluid. After this short time, and as soon as at least

one marked particle entered the window, particle tracking began. The experiment was terminated when the sedimentation front arrived 4 cm above the marked particle(s). Sufficient experiments were performed at each concentration to provide a statistically satisfactory data ensemble (see Sec. III for further information regarding the statistical analysis of data).

Additional experiments were performed to examine the settling velocity of a single sphere in the fluid (i.e., the case of infinitely dilute suspensions,  $\phi=0\%$ ). The sphere was placed into the top of the median plane of the vessel containing only the fluid. The sphere was then allowed to settle, and particle tracking began inside the two imaging windows as soon as the sphere reached the top of the upper window. The experiment ended when the sphere reached the bottom of the lower window.

### C. Particle tracking method

Particle tracking was performed with a real time digital imaging processing system. The system consisted of a miniature CCD video camera (XC-77CE,  $512 \times 512$  pixels) connected to a fast and intelligent image processing and acquisition board (Matrox Image 1280), located in a personal computer (Dell 466SE with an Intel 486 processor at 66 MHz) operating with digital imaging software (Visilog 4.1 by Noesis). The tracking in real time was achieved with a specially designed program, which used some of the software functions and was then included as a function into the software package. The program consisted of the following steps performed for a chosen number of loops, which depended on the average time for a particle to cross the imaging window(s) at a given concentration: image acquisition; image threshold for obtaining a binary image, where only the projections of the marked particles onto the window plane could be seen; small binary image erosion to suppress any small impurities, other than the particles; ultimate image erosion in order that particle projection centers are represented by isolated pixels; localization of the isolated pixels; and recording of the horizontal and vertical coordinates of the particle centers as well as the acquisition time into a file.

The experimental error in the particle center measurement was of the order of one pixel. The time between two image acquisitions, that is, the sampling time, had an average value of 2 s and varied slightly during particle settling, depending upon the speed of the different steps of the program. The sampling time was determined very accurately from the on-board real time image processor. Sampling problems can arise when the particles moved one pixel, which is the uncertainty in the particle center measurement, during the sampling time (also see Secs. IV B and IV C for a further discussion). This occurred, in particular, at large concentrations, where the particle settling speed was small. This "pixel noise" could be avoided by increasing the sampling time. However, there are problems in increasing it. Indeed, the sampling time should be kept much smaller than the correlation time (see Secs. III B and IV C). At large concentration, the simplest modification was just to use a larger magnification. A future possibility would be to use a center of mass after the small binary erosion instead of the ultimate erosion

in the program, because the former would have a resolution of 0.1 pixels. Considerable reprogramming would be needed, and the code could take much longer. Therefore, this possibility has not yet been explored. Finally, it should be mentioned that the sampling time (of the order of 2 s) was always smaller than the time a particle takes to traverse the recording window (at least of the order of 200 s).

The files that contained the horizontal and vertical coordinates,  $X_{\perp}$  and  $X_{\parallel}$  respectively, of the settling particles as function of time,  $t$ , were then analyzed with a spreadsheet software (Microsoft Excel 4.0). In the remainder of the paper, the indices  $\parallel$  and  $\perp$  denote quantities parallel and perpendicular to gravity.

## III. STATISTICAL DATA ANALYSIS

### A. Mean velocity and standard deviation

The first objective of this work was to compute mean velocities and velocity fluctuations. The main issue was to choose a correct statistical ensemble of data over which to average. Horizontal and vertical local velocities of a particle were calculated over each sampling time interval. For a given particle concentration, histograms of all local velocities were then examined. Mean and standard deviation,  $\langle V \rangle$  and  $\sigma_v$ , respectively, of the local velocities for all times and all tracked particles for this concentration were then determined. Both statistical and experimental errors were computed.

The statistical error in the mean was given by the standard error in the mean, with its familiar significance as the 68% confidence limit, which was defined as the standard deviation divided by the square root of the number of uncorrelated observations of the local velocities.<sup>26</sup> We assumed that the local velocities remain correlated only during the time for the velocity autocorrelation function to drop to the noise level, as estimated by the analysis described in Sec. III B. Typically, for each particle concentration, the number of uncorrelated local velocities was of the order of 500. The statistical ensemble was therefore found sufficient to produce meaningful statistics.

The experimental errors in the mean and standard deviation were also estimated by computing the usual propagation of errors in simple measurements, such as the particle coordinates and sampling time.<sup>26</sup> It should be mentioned that the experimental error in the local velocity can become large for high concentration with a small image magnification, since, in that last case, the particles moved about one pixel, which is the uncertainty in the particle center measurement, during the sampling time. This "pixel noise" has little effect on the mean velocity when averaging over a long time, but can produce artificially high fluctuations in the local velocity. Therefore, since the above method for computing standard deviations suffers a little from "pixel noise" at the higher concentrations, an alternative method is proposed in Sec. III B. It should be mentioned that since the experimental errors were always found to be larger than the statistical errors, they were considered the more representative.

Finally, it should be noted that the above analysis presumed the validity of the ergodic hypothesis since local ve-

locities of different particles were supposed statistically identical to local velocities of a single particle along its trajectory. Since it treated all observations equally, the analysis assumed that the system did not age during each trajectory.

## B. Velocity fluctuation autocorrelation functions

The second objective of this work was to determine the long time behavior of the fluctuating particle motions. This could be achieved by examining whether particle velocity became uncorrelated, and consequently by computing particle velocity fluctuation autocorrelation functions. The data reduction began with the computation of the local particle velocities sampled over a constant time interval for each particle. Since the sampling time slightly varied along a particle trajectory, the horizontal and vertical coordinates of each settling particle were linearly interpolated for constant time intervals. The constant time interval was chosen to be the mean sampling time,  $\Delta t = 2$  s. The horizontal and vertical local particle velocities were then calculated over each interval. The horizontal and vertical velocity fluctuation autocorrelation functions, denoted  $C(t)$  ( $C_{\perp}$  and  $C_{\parallel}$ , respectively), could therefore be computed as  $C(t) = \langle V'(t_0)V'(t_0+t) \rangle$  ensemble averaged over different particle trajectories and different starting times  $t_0$ . Here  $V' = V - \langle V \rangle$  is the local velocity fluctuation, where  $\langle V \rangle$  was taken as the mean (horizontal or vertical) velocity calculated for the chosen set of particles by means of the method described in Sec. III A. Typically, for each particle concentration, 30 particles were chosen with trajectories longer than a dimensionless time of 200 (based on time scale  $a/V_S$ ). A number of 30 particles was found sufficient to reduce noticeably the statistical fluctuations. In forming the velocity autocorrelation functions  $C(t)$ , we used for the starting times,  $t_0$ , all the different observation times for the selected trajectories. While there is little new information from all the starting times,  $t_0$ , within a correlation time, some random experimental noise is removed by treating all the observations equally. The errors in the correlation functions were given by the standard error in the mean, which was defined as the standard deviation divided by the square root of the number of uncorrelated data, that is, the 68% confidence limits.<sup>26</sup>

It was then possible to verify whether the autocorrelation functions were decaying in time. When the functions decreased toward zero, correlation times and self-diffusivities were estimated. Two methods were used to compute the correlation times. The first method (exponential fit method) could only be used when the function decayed as a single exponential in time, that is,  $C(t) = C(0) \exp(-t/t_c)$ . The logarithm of the function was fitted to a straight line with the method of weighted least squares<sup>26</sup> and the correlation time,  $t_c$  ( $t_{c\perp}$  and  $t_{c\parallel}$ ), was then deduced. The second method (integral method) could always be applied. It was based upon the definition of the correlation time as  $t_c = [1/C(0)] \int_0^{\infty} C(t) dt$ . Practically, the integration was performed from  $t=0$  to  $t=t_{\infty}$ , the time at which the autocorrelation function began to oscillate around zero (the oscillations are due to statistical fluctuations). Finally, self-diffusivities, denoted  $D$  ( $D_{\perp}$  and  $D_{\parallel}$ ), could be obtained in

terms of the correlation functions via  $D = \int_0^{\infty} C(t) dt$ , that is,  $D = C(0)t_c$ . Self-diffusivities were found by using the above two methods. The estimates of the errors in self-diffusivities are a combination of errors in simple measurements and statistical errors due to a finite number of observed particle trajectories.<sup>26</sup>

In order to treat all observations equally, a slightly different definition of the velocity correlation function was used in the calculation of this integral. The velocity fluctuation autocorrelation function was calculated as  $C(t) = \sum_{\text{trajectories}, t_0} V'(t_0+t)V'(t_0) / \sum_{\text{trajectories}}$  numbers of observations at  $t=0$ . This method of calculation prevents a few, uncertain observations at large separation times dominating the integral. For short separation  $t$ , the number of observation at  $t=0$  is not much different from that at  $t$ , and hence, this definition is not much different from the previous definition.

Finally, another method to estimate the velocity standard deviation is to compute the square root of the experimental value of  $C(0)$ , which is based on the subset of 30 particles with long trajectories. However, "pixel noise," which can be recognized to be present by a sharp initial drop in the velocity correlation is a problem at high concentrations (see Sec. IV C). This "pixel noise" can be avoided by using the extrapolated value of the exponential fit of  $C(t)$  back to  $t=0$  instead of the experimental value of  $C(0)$ . Again, the estimates of the errors are a combination of errors in simple measurements and statistical errors due to a finite number of observed particle trajectories.<sup>26</sup> It should be noted that "pixel noise" has a negligible effect on the diffusivity, as calculated as an integral over the velocity correlation function, because the contribution of the single erroneous initial point to the integral is very small.

## C. Second-order moments of the particle displacement

Another method to investigate the long time behavior of the fluctuating particle motions was to compute the second-order moment of the particle displacement. From the interpolated horizontal and vertical coordinates of the settling particles, the horizontal and vertical second-order moments of the particle displacement fluctuations, denoted  $M_2$  ( $M_{2\perp}$  and  $M_{2\parallel}$ , respectively), were calculated for a given particle concentration as  $M_2(t) = \langle [X(t_0+t) - X(t_0) - \langle V \rangle t]^2 \rangle$  ensemble averaged over different particle trajectories and different starting times  $t_0$ . The set of particles was chosen to be the same as that for the correlation function determination summarized in Sec. III B. The average  $\langle V \rangle$  was taken as the mean (horizontal or vertical) velocity calculated for this set of particles by means of the method described in Sec. III A. The uncertainties in the moments were given by the standard error in the mean, which was defined as the standard deviation divided by the square root of the number of uncorrelated data.<sup>26</sup> A diffusive behavior was characterized by a linear growth with time of the second-order moments after few correlation times. The second-order moments were fitted to a straight line with the method of weighted least squares<sup>26</sup> and the self-diffusivities were then extracted from the slope of this fitted line (the second-order moment method). It should

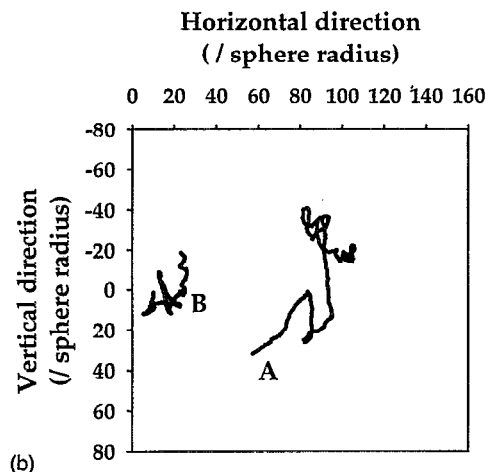
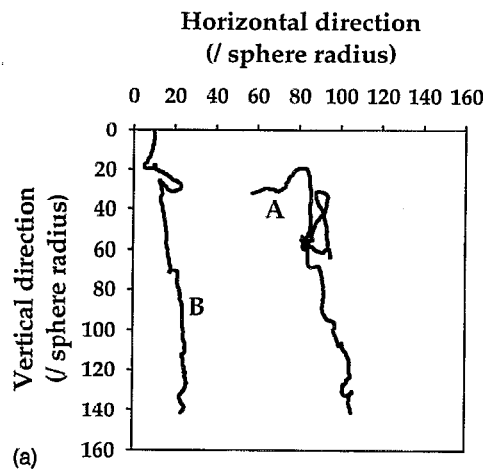


FIG. 1. Two typical trajectories in the laboratory reference frame (a) and same particle trajectories in the mean settling reference frame (b) for  $\phi=30\%$ .

be noted that this second-order moments method for evaluating the diffusivity is closely related to the correlation function method at the end of Sec. III B, which uses the modified correlation function. This method based on displacements is also insensitive to the problems of “pixel noise.”

#### IV. EXPERIMENTAL RESULTS

##### A. Particle trajectories

Two typical particle trajectories are presented in Fig. 1(a) for  $\phi=30\%$ . These trajectories are rather tortuous, and

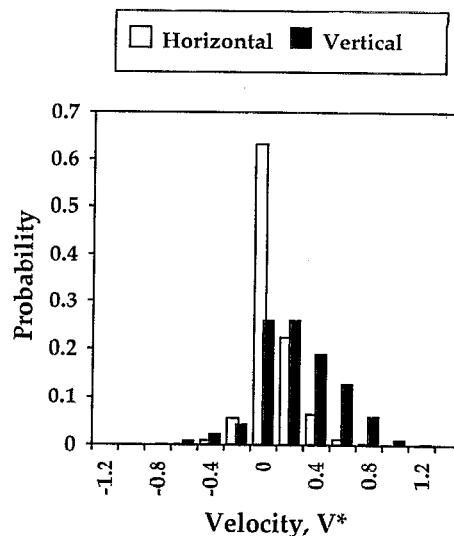


FIG. 2. Histograms of the horizontal and vertical velocity fluctuations for  $\phi=30\%$  (the velocities,  $V^*$ , are made dimensionless by scaling with  $V_S$ ).

exhibit large as well as small loops. In Fig. 1(b), trajectories of the same particles are displayed in the mean settling reference frame. The particle motion fluctuations are strongly anisotropic, with vertical fluctuations much larger than horizontal fluctuations. The particle trajectories relative to the mean velocity demonstrate graphically that there are several independent events, i.e., that the data are sufficiently long in time to observe a long time behavior.

##### B. Mean velocities and velocity fluctuations

Histograms of the velocities are all found to be very smooth and approximately Gaussian, as illustrated for  $\phi=30\%$  in Fig. 2, and therefore to be well represented by the mean and the variance. Table I presents the measured dependence of the dimensionless horizontal and vertical mean velocities,  $\langle V_{\perp} \rangle^*$  and  $\langle V_{\parallel} \rangle^*$ , and the standard deviations,  $\sigma_{v_{\perp}}^*$  and  $\sigma_{v_{\parallel}}^*$ , upon the particle concentration. All the values have been made dimensionless by scaling with the Stokes' velocity of an isolated sphere calculated with the Stokes' formula given in the introduction,  $V_S=0.037\pm 0.005$  cm/s (the error bar is mainly due to particle size dispersion). The measured mean vertical velocity of an isolated sphere ( $\phi=0\%$ ) is  $0.038\pm 0.001$  cm/s, in good agreement with the theoretical value

TABLE I. Dimensionless horizontal and vertical mean velocities,  $\langle V_{\perp} \rangle^*$  and  $\langle V_{\parallel} \rangle^*$ , and standard deviations,  $\sigma_{v_{\perp}}^*$  and  $\sigma_{v_{\parallel}}^*$ . The results are made dimensionless by scaling with the theoretical value of the Stokes' velocity,  $V_S$ .

| $\phi$                            |                           | $0.050\pm 0.001$ | $0.100\pm 0.001$ | $0.150\pm 0.002$ | $0.200\pm 0.003$ | $0.250\pm 0.003$ | $0.300\pm 0.004$ | $0.350\pm 0.004$   | $0.400\pm 0.005$  |
|-----------------------------------|---------------------------|------------------|------------------|------------------|------------------|------------------|------------------|--------------------|-------------------|
| $\langle V_{\perp} \rangle^*$     | From all local velocities | $0.06 \pm 0.03$  | $0.01 \pm 0.05$  | $0.01 \pm 0.02$  | $0.02 \pm 0.03$  | $0.00 \pm 0.02$  | $0.00 \pm 0.02$  | $-0.005 \pm 0.009$ | $0.006 \pm 0.009$ |
| $\langle V_{\parallel} \rangle^*$ | From all local velocities | $0.8 \pm 0.1$    | $0.7 \pm 0.1$    | $0.57 \pm 0.08$  | $0.39 \pm 0.06$  | $0.29 \pm 0.04$  | $0.17 \pm 0.03$  | $0.14 \pm 0.02$    | $0.07 \pm 0.01$   |
| $\sigma_{v_{\perp}}^*$            | From all local velocities | $0.33 \pm 0.04$  | $0.35 \pm 0.05$  | $0.32 \pm 0.04$  | $0.24 \pm 0.03$  | $0.24 \pm 0.03$  | $0.19 \pm 0.03$  | $0.14 \pm 0.02$    | $0.07 \pm 0.01$   |
| $\sigma_{v_{\perp}}^*$            | From experimental $C(0)$  | $0.27 \pm 0.04$  | $0.31 \pm 0.05$  | $0.28 \pm 0.04$  | $0.21 \pm 0.03$  | $0.19 \pm 0.03$  | $0.16 \pm 0.02$  | $0.12 \pm 0.02$    | $0.06 \pm 0.01$   |
| $\sigma_{v_{\perp}}^*$            | From extrapolated $C(0)$  | $0.27 \pm 0.04$  | $0.31 \pm 0.04$  | $0.29 \pm 0.04$  | $0.21 \pm 0.03$  | $0.17 \pm 0.02$  | $0.15 \pm 0.02$  | $0.11 \pm 0.01$    | $0.05 \pm 0.01$   |
| $\sigma_{v_{\parallel}}^*$        | From all local velocities | $0.62 \pm 0.08$  | $0.68 \pm 0.09$  | $0.61 \pm 0.08$  | $0.44 \pm 0.06$  | $0.39 \pm 0.05$  | $0.29 \pm 0.04$  | $0.19 \pm 0.03$    | $0.09 \pm 0.01$   |
| $\sigma_{v_{\parallel}}^*$        | From experimental $C(0)$  | $0.51 \pm 0.08$  | $0.61 \pm 0.09$  | $0.54 \pm 0.08$  | $0.37 \pm 0.06$  | $0.34 \pm 0.05$  | $0.26 \pm 0.04$  | $0.17 \pm 0.03$    | $0.08 \pm 0.01$   |
| $\sigma_{v_{\parallel}}^*$        | From extrapolated $C(0)$  | $0.54 \pm 0.08$  | $0.65 \pm 0.09$  | $0.57 \pm 0.08$  | $0.38 \pm 0.05$  | $0.34 \pm 0.05$  | $0.27 \pm 0.04$  | $0.17 \pm 0.02$    | $0.07 \pm 0.01$   |

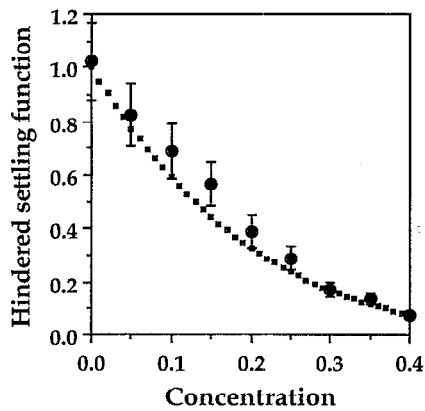


FIG. 3. Hindered settling function. The solid circles are the experimental data and the dotted curve corresponds to the Richardson-Zaki law with  $n=5$ .

of the Stokes' velocity,  $V_S$ , within the uncertainty range. The measured mean horizontal velocities are zero within error bars.

The experimental dimensionless settling speeds,  $\langle V_{\parallel} \rangle^*$ , decrease with  $\phi$ , as displayed in Fig. 3. The logarithm of the experimental hindered settling function has been fitted to a linear function of the logarithm of  $1-\phi$  by the method of weighted least squares.<sup>26</sup> A Richardson-Zaki<sup>7</sup> law,  $f(\phi) = (1-\phi)^n$ , with  $n = 5.0 \pm 0.3$  is in fairly good agreement with the experimental data (the correlation coefficient of the linear fit is 0.99).

The horizontal and vertical velocity fluctuations,  $\sigma_{v\perp}^*$  and  $\sigma_{v\parallel}^*$ , have been determined by means of the three methods described in Secs. III A and III B. The velocity fluctuations estimated by these three methods match within error bars. However, since "pixel noise" contributes a small systematic erroneous increase for the two first methods at high concentration, the numbers deduced from the extrapolated value of  $C(0)$  are quoted for the values of the fluctuations at  $\phi=35\%$  and  $40\%$  in the remainder of this paper. It should be

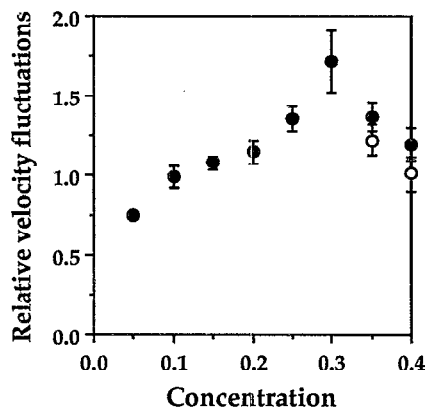


FIG. 4. The vertical relative velocity fluctuations,  $\sigma_{v\parallel}/\langle V_{\parallel} \rangle$ , vs  $\phi$ . The solid circles are the experimental data computed from the local velocities and the open circles from the extrapolated values of  $C(0)$ .

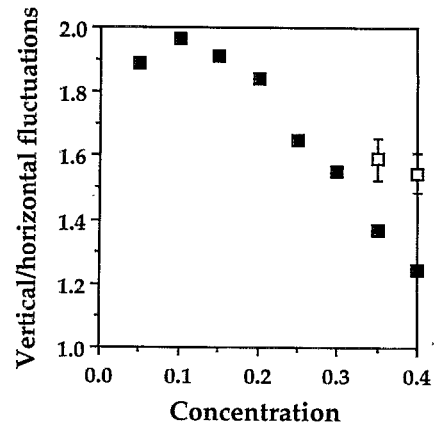


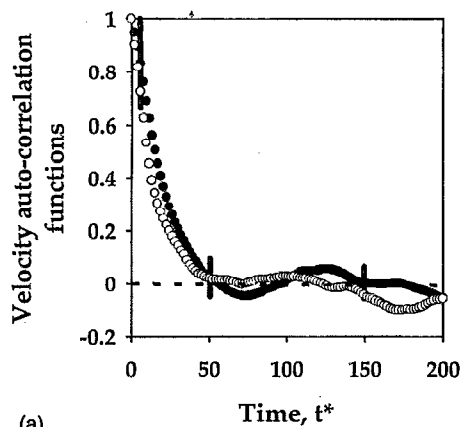
FIG. 5. The ratio between the vertical and horizontal standard deviations,  $\sigma_{v\parallel}/\sigma_{v\perp}$ , vs  $\phi$ . The solid squares are the experimental data computed from the local velocities and the open squares from the extrapolated values of  $C(0)$ .

mentioned that an important part of the error in dimensionless standard deviation comes from the error in Stokes' velocity.

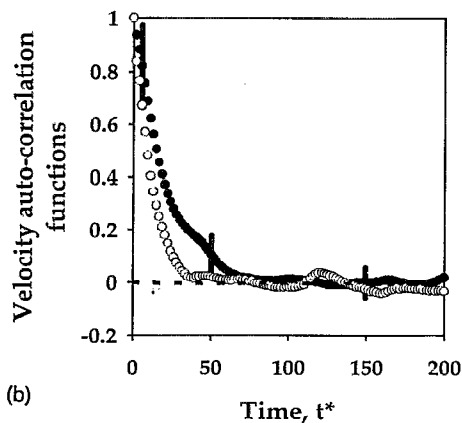
The velocity fluctuations also decrease with concentration. In order to examine the importance of the velocity fluctuations, the relative velocity fluctuations in the vertical,  $\sigma_{v\parallel}/\langle V_{\parallel} \rangle$ , are plotted versus  $\phi$  in Fig. 4. Clearly, the relative fluctuations are large, ranging between  $0.75 \pm 0.01$  and  $1.7 \pm 0.3$ . The relative vertical velocity fluctuations increase at low concentration, reach a maximum of  $1.7 \pm 0.3$  at  $\phi=30\%$  and then decrease at higher concentration. The ratio between the vertical and horizontal standard deviations,  $\sigma_{v\parallel}/\sigma_{v\perp}$ , which characterizes the anisotropy of the velocity fluctuations, is plotted versus  $\phi$  in Fig. 5. This ratio is approximately 1.9 for low concentration and then decreases with increasing concentration, to reach a value of about 1.6 for  $\phi=40\%$ . In order to show the effect of "pixel noise" at high concentrations, data computed from the local velocities, and from the extrapolated values of  $C(0)$  have been plotted for  $\phi=35\%$  and  $40\%$  in Figs. 4 and 5. It should be noticed that the error bars for this last method are large, since they correspond to statistical errors due to a small number (typically 30) of observed trajectories.

### C. Velocity autocorrelation functions and correlation times and lengths

Normalized velocity fluctuation autocorrelation functions,  $C(t^*)/C(0)$ , for both horizontal and vertical directions, are shown in Fig. 6 for three different particle concentrations. In these curves, the time,  $t^*$ , has been made dimensionless by scaling with the Stokes' time,  $a/V_S$ . The correlation functions always decrease as a single exponential toward zero, which demonstrates that particle velocity always become uncorrelated. Moreover, the velocities seem to become uncorrelated around a dimensionless time  $t^*=60$  for all concentrations. In all cases, when the functions approach zero, the oscillations around zero are due to statistical noise. In addition, the horizontal and vertical correlation functions



(a)



(b)

have a similar relaxation. As a general trend, the decay of the vertical correlation functions is slightly slower than that of the horizontal correlation functions. It should also be mentioned that the large image magnification was needed at  $\phi=40\%$ . Indeed, when the small magnification was used, both correlation functions experience a sharp decrease to zero at early times, which is not as strong as that for the large magnification. This short time jump is the sign of “pixel noise” due to sampling problems mentioned in Sec. II C. Such small jumps can, in fact, be seen in Fig. 6(c), with a drop of 30% for the vertical motion and 43% for the horizontal

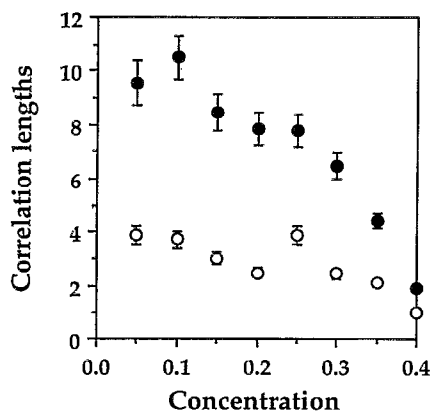


FIG. 7. The dimensionless horizontal and vertical correlation lengths,  $l_{c\perp}^*$  and  $l_{c\parallel}^*$ , vs  $\phi$ . The solid circles are the experimental data for the vertical direction and the open circles for the horizontal direction.

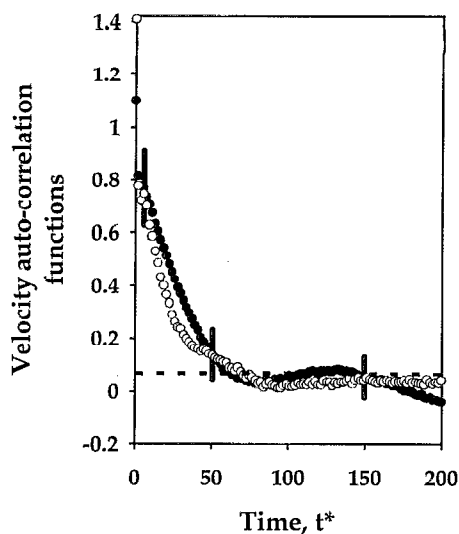


FIG. 6. Normalized velocity fluctuation autocorrelation functions for  $\phi=5\%$  (a), 20% (b), and 40% (c). The solid circles are the experimental data for the vertical functions and the open circles for the horizontal functions. The uncertainty range is indicated for three data points on the vertical functions (the same uncertainty range is obtained for the horizontal functions).

zonal motion at  $\phi=40\%$ . Smaller jumps are also discernible at  $\phi=35\%$ , but do not occur at lower concentrations. As mentioned in Secs. III B and IV B, this “pixel noise” can be avoided by using the extrapolated value of  $C(t)$  back to  $t=0$ . These corrected values of  $C(0)$  were used to compute the correlation times and lengths in Table II and Fig. 7, and to normalize the velocity autocorrelation functions at  $\phi=35\%$  and 40%.

Table II presents the dimensionless correlation times,  $t_{c\perp}^*$  and  $t_{c\parallel}^*$  (based on time scale  $a/V_S$ ), determined by means of the integral method and the exponential fit method described in Sec. III B (the correlation coefficients of the fit are better than 0.99). The correlation times estimated with both methods match within error bars. As a general trend, the correlation time seems independent of concentration and vertical times are slightly longer than horizontal times. It should be noted that, for all experiments, the correlation times are larger than the measurement sampling time ( $\approx 2$  s), thereby ensuring a statistically correct sampling of data.

A correlation length can be roughly estimated by  $t_c \sigma_v = D / \sigma_v = (t_c D)^{1/2}$ , where the interrelated quantities,  $t_c, \sigma_v [=C(0)^{1/2}]$  and  $D$ , are computed using the same statistical ensemble of data (see Sec. III B). It should be noted that this correlation length is the distance the particle moves with the fluctuation of the velocity while the velocity remains correlated, and is not the spatial correlation length. The dimensionless vertical and horizontal correlation lengths,  $l_{c\perp}^*$  and  $l_{c\parallel}^*$  (based on length scale  $a$ ), both decrease with  $\phi$ , as shown in Table II and Fig. 7, where the correlation lengths estimated from the integral method are plotted versus

TABLE II. Dimensionless horizontal and vertical correlation times,  $t_{c\perp}^*$  and  $t_{c\parallel}^*$ , and correlation lengths,  $l_{c\perp}^*$  and  $l_{c\parallel}^*$ . The results are made dimensionless by scaling with the time  $a/V_S$  and with the length  $a$ .

| $\phi$             |                        | $0.050 \pm 0.001$ | $0.100 \pm 0.001$ | $0.150 \pm 0.002$ | $0.200 \pm 0.003$ | $0.250 \pm 0.003$ | $0.300 \pm 0.004$ | $0.350 \pm 0.004$ | $0.400 \pm 0.005$ |
|--------------------|------------------------|-------------------|-------------------|-------------------|-------------------|-------------------|-------------------|-------------------|-------------------|
| $t_{c\perp}^*$     | Exponential fit method | $14 \pm 3$        | $12 \pm 2$        | $11 \pm 2$        | $12 \pm 2$        | $24 \pm 4$        | $17 \pm 3$        | $20 \pm 3$        | $23 \pm 4$        |
| $t_{c\perp}^*$     | Integral method        | $15 \pm 3$        | $12 \pm 2$        | $11 \pm 2$        | $12 \pm 2$        | $20 \pm 4$        | $16 \pm 3$        | $20 \pm 3$        | $22 \pm 4$        |
| $t_{c\parallel}^*$ | Exponential fit method | $18 \pm 3$        | $16 \pm 3$        | $16 \pm 3$        | $21 \pm 3$        | $27 \pm 4$        | $25 \pm 4$        | $25 \pm 4$        | $28 \pm 5$        |
| $t_{c\parallel}^*$ | Integral method        | $19 \pm 4$        | $17 \pm 3$        | $16 \pm 3$        | $21 \pm 4$        | $23 \pm 4$        | $25 \pm 5$        | $26 \pm 4$        | $26 \pm 4$        |
| $l_{c\perp}^*$     | Exponential fit method | $3.9 \pm 0.4$     | $3.8 \pm 0.3$     | $3.2 \pm 0.3$     | $2.5 \pm 0.2$     | $4.3 \pm 0.3$     | $2.6 \pm 0.2$     | $2.1 \pm 0.2$     | $1.1 \pm 0.1$     |
| $l_{c\perp}^*$     | Integral method        | $3.9 \pm 0.4$     | $3.7 \pm 0.3$     | $3.0 \pm 0.2$     | $2.5 \pm 0.2$     | $3.9 \pm 0.4$     | $2.4 \pm 0.2$     | $2.1 \pm 0.1$     | $1.0 \pm 0.1$     |
| $l_{c\parallel}^*$ | Exponential fit method | $9.8 \pm 0.8$     | $10.5 \pm 0.8$    | $8.9 \pm 0.7$     | $8.1 \pm 0.6$     | $9.2 \pm 0.6$     | $6.6 \pm 0.5$     | $4.3 \pm 0.3$     | $2.1 \pm 0.2$     |
| $l_{c\parallel}^*$ | Integral method        | $9.5 \pm 0.8$     | $10.5 \pm 0.8$    | $8.4 \pm 0.7$     | $7.8 \pm 0.6$     | $7.8 \pm 0.6$     | $6.5 \pm 0.5$     | $4.5 \pm 0.3$     | $1.9 \pm 0.1$     |

$\phi$ . The vertical correlation length is always larger than the horizontal correlation length. However, this anisotropy decreases with increasing concentration. At large concentration, the correlation lengths are of the order of a particle radius. It should be noted that the correlation length is always much smaller than the vessel inner width.

#### D. Hydrodynamic self-diffusivities

The diffusive behavior of the particle motion fluctuations can be established by two means, as described in Sec. III. First, study of the velocity correlation functions shows that the particle velocity becomes uncorrelated at all concentrations. Integrals of the correlation functions always reach saturation values, which are defined as the self-diffusivities, around  $t^* = 60$ , as illustrated for  $\phi = 30\%$  in Fig. 8. The integrals are made dimensionless with a length scale  $a$  and a time scale  $a/V_S$ . Second, second-order moments of the particle displacement fluctuations always grow linearly with time after a few correlation times, i.e., after the first curved part, for all concentrations (the correlation coefficients of the linear fit described in Sec. III C are better than 0.99). This behavior is illustrated for  $\phi = 30\%$  in Fig. 9, where the

second-order moments are made dimensionless by scaling with the length scale  $a$ .

Table III gives the dimensionless self-diffusivities,  $D_{\perp}^*$  and  $D_{\parallel}^*$  (based on length scale  $a$  and time scale  $a/V_S$ ), determined by means of the three methods described in Sec. III. The self-diffusivities estimated with the different methods match within error bars. The diffusion process is strongly anisotropic. Vertical self-diffusivities are larger than horizontal self-diffusivities, as seen clearly in Figs. 8 and 9. Again, this anisotropy decreases with increasing concentration. Vertical and horizontal self-diffusivities decrease with particle concentration, as displayed in Fig. 10, where the self-diffusivities estimated from the integral method are plotted versus  $\phi$ . It should be noted that the datum for  $\phi = 5\%$  is slightly smaller than that for  $\phi = 10\%$ . However, because of the large error bar, it is difficult to say whether this corresponds to a significant trend. Another scaling can be built with the time scale  $a/\langle V_{\parallel} \rangle$ , which uses the mean settling velocity in place of the Stokes' velocity. The self-diffusivities made dimensionless with this alternative scaling seem to be independent of concentration over a substantial concentration range, in which the mean velocity varies by a factor of

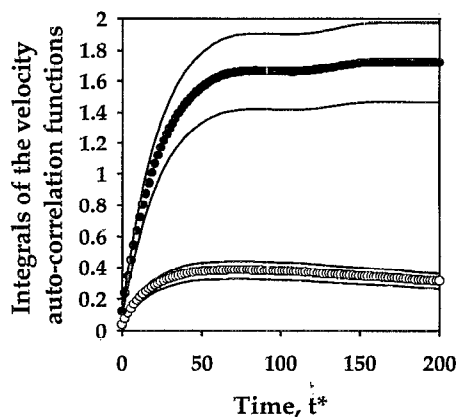


FIG. 8. Dimensionless integrals of the velocity autocorrelation functions for  $\phi = 30\%$ . The solid circles are the experimental data for the vertical direction and the open circles for the horizontal direction. The solid lines indicate the 68% confidence limit.

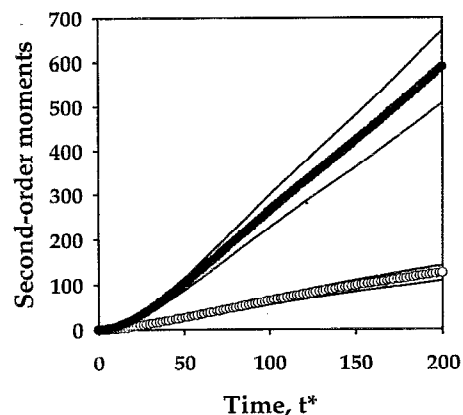


FIG. 9. Dimensionless second-order moments of the particle displacement fluctuations for  $\phi = 30\%$ . The solid circles are the experimental data for the vertical direction and the open circles for the horizontal direction. The solid lines indicate the 68% confidence limit.

TABLE III. Dimensionless horizontal and vertical self-diffusivities,  $D_{\perp}^*$  and  $D_{\parallel}^*$ . The results are made dimensionless by scaling with  $aV_S$ .

| $\phi$            |                            | 0.050±0.001 | 0.100±0.001 | 0.150±0.002 | 0.200±0.003 | 0.250±0.003 | 0.300±0.004 | 0.350±0.004 | 0.400±0.005 |
|-------------------|----------------------------|-------------|-------------|-------------|-------------|-------------|-------------|-------------|-------------|
| $D_{\perp}^*$     | Second-order moment method | 0.9±0.1     | 1.0±0.1     | 0.9±0.1     | 0.5±0.1     | 0.7±0.1     | 0.4±0.1     | 0.21±0.03   | 0.04±0.01   |
| $D_{\perp}^*$     | Exponential fit method     | 1.1±0.2     | 1.2±0.2     | 0.9±0.2     | 0.5±0.1     | 0.8±0.1     | 0.4±0.1     | 0.23±0.04   | 0.05±0.01   |
| $D_{\parallel}^*$ | Integral method            | 1.0±0.2     | 1.1±0.2     | 0.9±0.1     | 0.5±0.1     | 0.8±0.1     | 0.4±0.1     | 0.23±0.03   | 0.05±0.01   |
| $D_{\parallel}^*$ | Second-order moment method | 4.6±0.7     | 6.4±0.9     | 4.2±0.6     | 2.6±0.4     | 2.6±0.4     | 1.6±0.2     | 0.8±0.1     | 0.15±0.02   |
| $D_{\parallel}^*$ | Exponential fit method     | 5.3±1.0     | 6.8±1.2     | 5.1±0.9     | 3.1±0.5     | 3.2±0.5     | 1.8±0.3     | 0.7±0.1     | 0.15±0.03   |
| $D_{\parallel}^*$ | Integral method            | 4.9±0.7     | 6.4±1.0     | 4.5±0.7     | 2.9±0.4     | 2.7±0.4     | 1.7±0.2     | 0.8±0.1     | 0.14±0.02   |

5, as shown in Fig. 11. The self-diffusivities decrease in this scaling above  $\phi=30\%$ .

### V. DISCUSSIONS AND CONCLUDING REMARKS

In this work, the motion of sedimenting non-Brownian spheres has been examined experimentally at low Reynolds numbers. A few marked spheres were tracked in the bulk of the suspension of like spheres, using a real time digital imaging processing system. Particle trajectories were examined for particle concentrations ranging from 0% to 40% in 5% steps, and a statistical analysis of local particle velocities was performed.

The experimentally inferred hindered settling function was found to be in fairly good agreement with a Richardson-Zaki law,  $f(\phi) = (1 - \phi)^n$  with  $n = 5.0 \pm 0.3$ . Although the velocity of the sedimentation front and the average settling speed in the bulk of the suspension are not expected to be exactly the same, the same order of magnitude for the index  $n$  is found in the present measurements as in previous determinations of the sedimentation front speed.<sup>1</sup> An index of order 5 has also been obtained in numerical simulations.<sup>20</sup> Experiments by Ham and Homsey<sup>6</sup> for a slightly lower concentration range ( $2.5\% \leq \phi \leq 10\%$ ) gave a lower value of  $n$ , which was attributed to structure development that arose even in initially well-mixed suspensions. In

the present measurements, the mean horizontal velocity has been found equal to zero within experimental uncertainty. This finding confirms that the experiments were not perturbed by any mean convective flow.

The fluctuations in settling speed have been found to be large, ranging between 75% and 170% of the mean. The relative fluctuations increase at low concentrations to reach a maximum value of 170% at  $\phi=30\%$  and then decrease at higher concentrations. It has indeed been presumed that they vary between zero at  $\phi=0\%$ , where a particle is isolated, and zero again at close packing ( $\phi \approx 60\%$ ), and to present a maximum in between.<sup>22</sup> The present experimental estimates of the vertical velocity fluctuations are larger than those of Ham and Homsey<sup>6</sup> (=46% of the mean for  $\phi=5\%$ ), though still less than the theoretical prediction of Koch and Shaqfeh<sup>17</sup> (=2.2 $V_S$ ). They are also of the same order of magnitude as the results of the experiments of Xue *et al.*<sup>8</sup> The decrease of the relative velocity fluctuations above  $\phi=30\%$  in these later experiments is, however, much stronger than in the present experiments. In addition, in the present work, the velocity fluctuations have been found to be strongly anisotropic. Vertical fluctuations are approximately twice as large as horizontal fluctuations for  $5\% \leq \phi \leq 15\%$ . The anisotropy in velocity fluctuation decreases with further increasing concentration.

The diffusive behavior of the fluctuating particle motion

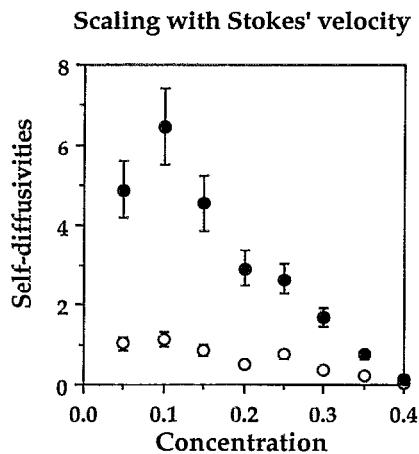


FIG. 10. The horizontal and vertical self-diffusivities made dimensionless by scaling with  $aV_S$  vs  $\phi$ . The solid circles are the experimental data for the vertical direction and the open circles for the horizontal direction.

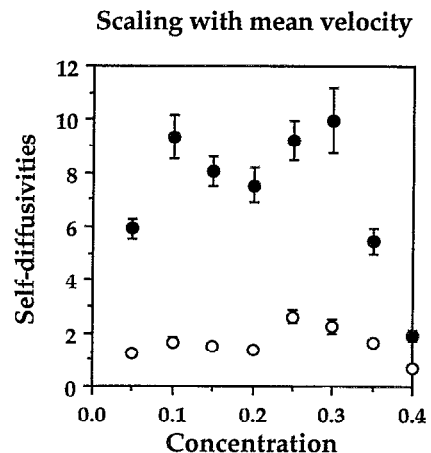


FIG. 11. The horizontal and vertical self-diffusivities made dimensionless by scaling with  $a\langle V_{\parallel} \rangle$  vs  $\phi$ . The solid circles are the experimental data for the vertical direction and the open circles for the horizontal direction.

has been demonstrated by examining the relaxation of the particle velocity autocorrelation functions, as well as by studying the second-order moments of the particle displacements. This finding confirms and extends the results of Ham and Homsy.<sup>6</sup> Vertical and horizontal correlation times and lengths, as well as vertical and horizontal self-diffusivities have been found as a function of  $\phi$ . The measured correlation times are independent of the concentration. The vertical times are slightly larger than the horizontal times. The self-diffusivities decrease with increasing concentration. Since by definition the self-diffusivity is the product of the correlation time with the velocity variance, the self-diffusivity decreases with concentration like the variance. Moreover, the self-diffusivities normalized on the measured mean vertical velocity are constant over a substantial range of concentration in which the mean varies. These findings seem to suggest that the correct scaling would be to use the mean settling velocity. It should be noted that this scaling is more subtle, in that the velocity fluctuations do not scale with the mean velocity, and the correlation length is not constant. The present work also shows the strong anisotropy of the diffusion process in a fashion similar to other problems, e.g., hydrodynamic dispersion in porous media. Again, this anisotropy decreases with concentration.

These experimental findings are different from the numerical results of Ladd,<sup>20</sup> who found a very large difference of time scales for horizontal and vertical velocity autocorrelation functions. In a recent work, Koch<sup>27</sup> examined the role of the vertical periodic boundaries on the diffusion process for box-size limited sedimenting point particles. The above difference in time scales was attributed to the periodic boundaries imposed in the vertical direction in the cubic-box numerical simulation, which do not exist in the present experiments with an oblong vessel. Some recent numerical simulations in Cambridge<sup>28</sup> of point particles sedimenting in a periodic box have suggested that an impenetrable lower boundary is important in reducing the vertical–horizontal anisotropy to realistic proportions.

The present vertical self-diffusivity is of the same order of magnitude as the result of the experiments of Ham and Homsy<sup>6</sup> ( $D_{\parallel} \approx 6aV_S$ ) for  $\phi=5\%$ . The decrease of the self-diffusivity with increasing concentration in the Ham and Homsy experiments is, however, stronger than in the present experiments. The present experimental value of the vertical self-diffusivity for  $\phi=5\%$  is also close to the value predicted by the hydrodynamic screening theory<sup>17</sup> ( $D_{\parallel}=0.52aV_S\phi^{-1}=10.4aV_S$ ). Koch<sup>27</sup> recently showed that a much larger value of the self-diffusivity was obtained for box-size limited point particles in a large aspect ratio cell, but again this may be due to the lack of an impenetrable lower boundary.<sup>28</sup> To complete this discussion, it should be also mentioned that the vertical self-diffusivity at low concentrations is of the same order of magnitude as that determined from the monolayer simulation of Lester.<sup>29</sup>

An interesting finding of the present work is the decrease of self-diffusivities and anisotropy for large concentrations. The following considerations can give some clues to this behavior. At large particle concentration, the hindrance is very high, and a particle is locked into a settling cluster of

particles. The basic mechanism for diffusion may be the fluctuating motion of clusters instead of the fluctuating motion of single particles. Collective motion of small clusters has been observed for a high concentration in the numerical simulations of Ladd.<sup>19</sup> In the present experiments, video recordings of the sedimenting suspension show very strong local fluctuations of the concentration. Additional experimental and theoretical work is necessary to understand thoroughly this large concentration regime, as well as the dependence of the self-diffusivities and correlation times with concentration.

Finally, since all the experiments were performed in the same size vessel, the problem of whether the velocity fluctuations and self-diffusivities vary with the vessel size, as has been suggested by some theories,<sup>15,16</sup> was not specifically addressed in the present paper. However, the estimated correlation lengths are always much smaller than the vessel inner width. This consideration seems to suggest that the experiments would not be affected by the vessel size. Additional experiments are, however, needed to give a definite answer to this question. This problem is examined in another study, where the inner vessel width is varied.<sup>30</sup>

## ACKNOWLEDGMENTS

We wish to thank G. M. Homsy for numerous useful discussions. We also like to thank L. de Arcangelis, J.-C. Charmet, H. Puhl, and S. Roux for valuable help and O. Brouard and D. Vallet for technical assistance. This work benefited from the stay of K.-V. Pham in our laboratory. The Santizicer 278 was donated by Monsanto and the glass beads were supplied by J.-C. Borgotti (Laboratoire Central des Ponts et Chaussées). The silvering technique was provided by C. Prost (Université de Nancy 1). This work was undertaken under the auspices of a CNRS-NSF cooperative research on hydrodynamics of fluid-particle systems and was partially supported by Dowell Schlumberger Etudes et Fabrication. This work is part of the thesis of H. Nicolai sponsored by the Ministère de l'Enseignement Supérieur et de la Recherche.

<sup>1</sup>R. H. Davis and A. Acrivos, "Sedimentation of noncolloidal particules at low Reynolds numbers," *Annu. Rev. Fluid Mech.* **17**, 91 (1985).

<sup>2</sup>R. H. Davis and M. A. Hassen, "Spreading of the interface at the top of a slightly polydisperse sedimenting suspension," *J. Fluid Mech.* **196**, 107 (1988); R. H. Davis and M. A. Hassen, "Corrigendum," *J. Fluid Mech.* **202**, 598 (1989).

<sup>3</sup>J.-C. Bacri, C. Frénois, M. Hoyos, R. Perzynski, N. Rakotomalala, and D. Salin, "Acoustic study of suspension sedimentation," *Europhys. Lett.* **2**, 123 (1986).

<sup>4</sup>S. Lee, Y. Jang, C. Choi, and T. Lee, "Combined effect of sedimentation velocity fluctuation and self-sharpening on interface broadening," *Phys. Fluids A* **4**, 2601 (1992).

<sup>5</sup>D. Bruneau, R. Anthore, F. Feuillebois, X. Auvray, and C. Petipas, "Measurement of the average velocity of sedimentation in a dilute polydisperse suspension of spheres," *J. Fluid Mech.* **221**, 577 (1990).

<sup>6</sup>J. M. Ham and G. M. Homsy, "Hindered settling and hydrodynamic dispersion in quiescent sedimenting suspensions," *Int. J. Multiphase Flow* **14**, 533 (1988).

<sup>7</sup>J. F. Richardson and W. N. Zaki, "Sedimentation and fluidization: Part I," *Trans. Inst. Chem. Eng.* **32**, 35 (1954).

<sup>8</sup>J.-Z. Xue, E. Helbolzheimer, M. A. Rutgers, W. B. Russel, and P. M. Chaikin, "Diffusion, dispersion, and settling of hard spheres," *Phys. Rev. Lett.* **69**, 1715 (1992).

<sup>9</sup>G. K. Batchelor, "Sedimentation in a dilute dispersion of spheres," *J. Fluid Mech.* **52**, 245 (1972).

- <sup>10</sup>F. Feuillebois, "Sedimentation in a dispersion with vertical inhomogeneities," *J. Fluid. Mech.* **139**, 145 (1984).
- <sup>11</sup>E. J. Hinch, "An averaged-equation approach to particle interaction in a fluid suspension," *J. Fluid Mech.* **83**, 695 (1977).
- <sup>12</sup>P. G. Saffman, "On the settling speeds of free and fixed suspensions," *Stud. Appl. Math.* **52**, 115 (1973).
- <sup>13</sup>C. W. J. Beenaker, W. van Saarloos, and P. Mazur, "Many-sphere hydrodynamic interactions III: The influence of a plane wall," *Physica A* **127**, 451 (1984).
- <sup>14</sup>P. Nozières, "A local coupling between sedimentation and convection: Application to the Beenaker–Mazur effect," *Physica A* **147**, 219 (1987).
- <sup>15</sup>R. E. Caflisch and J. H. C. Luke, "Variance in the sedimentation speed of a suspension," *Phys. Fluids* **28**, 259 (1985).
- <sup>16</sup>E. J. Hinch, "Sedimentation of small particles," in *Disorder and Mixing*, edited by E. Guyon, J. P. Nadal, and Y. Pomeau (Kluwer Academic, Dordrecht, 1985), p. 153.
- <sup>17</sup>D. L. Koch and E. S. G. Shaqfeh, "Screening in sedimenting suspensions," *J. Fluid Mech.* **224**, 275 (1991).
- <sup>18</sup>J. F. Brady and G. Bossis, "Stokesian dynamics," *Annu. Rev. Fluid Mech.* **20**, 111 (1988).
- <sup>19</sup>R. E. Caflisch, C. Lim, J. H. C. Luke, and A. S. Sangani, "Periodic solutions for three sedimenting spheres," *Phys. Fluids* **31**, 3175 (1988).
- <sup>20</sup>A. J. C. Ladd, "Dynamical simulations of sedimenting spheres," *Phys. Fluids A* **5**, 299 (1993).
- <sup>21</sup>R. A. Keiller, "The spreading of the upper interface of a sedimenting monodisperse suspension," Report of the Laboratoire d'Aérothermique du CNRS, Meudon, 1992.
- <sup>22</sup>G. K. Batchelor, "A new theory of the instability of a uniform fluidized bed," *J. Fluid Mech.* **193**, 75 (1988).
- <sup>23</sup>J. M. Ham, S. Thomas, E. Guazzelli, G. M. Homsy, and M.-C. Anselmet, "An experimental study of the stability of liquid fluidized beds," *Int. J. Multiphase Flow* **16**, 171 (1990).
- <sup>24</sup>E. C. Eckstein, D. G. Bailey, and A. H. Shapiro, "Self-diffusion of particles in shear flow of a suspension," *J. Fluid Mech.* **79**, 191 (1977).
- <sup>25</sup>D. Leighton and A. Acrivos, "Measurement of shear-induced self-diffusion in concentrated suspensions of spheres," *J. Fluid Mech.* **177**, 109 (1987).
- <sup>26</sup>J. R. Taylor, "An introduction to error analysis," *University Science Books* (Oxford University Press, Oxford, 1982).
- <sup>27</sup>D. L. Koch, "Hydrodynamic diffusion in a suspension of sedimenting point particles with periodic boundary conditions," *Phys. Fluids* **6**, 2894 (1994).
- <sup>28</sup>F. R. da Cunha and E. J. Hinch (private communication).
- <sup>29</sup>J. C. Lester, "Hydrodynamic dispersion in concentrated sedimenting suspension," Ph.D. thesis, California Institute of Technology, 1988.
- <sup>30</sup>H. Nicolai and E. Guazzelli, "Effect of the vessel size on the hydrodynamic diffusion of sedimenting spheres," *Phys. Fluids* **7**, 3 (1995).